



# Biodegradable films functionalized with *Moringa oleifera* applied in food packaging

Adriana Gomes Verdi<sup>1</sup> · Alana Gabrieli de Souza<sup>1</sup> · Daniel Belchior Rocha<sup>1</sup> · Sueli Aparecida de Oliveira<sup>1</sup> · Rosa Maria Vercelino Alves<sup>2</sup> · Derval dos Santos Rosa<sup>1</sup>

Received: 1 June 2020 / Accepted: 10 November 2020 / Published online: 24 November 2020  
© Iran Polymer and Petrochemical Institute 2020

## Abstract

Biodegradable polymers are a suitable alternative for replacing traditional food packaging with environmental concerns. Poly(butylene adipate-*co*-terephthalate) (PBAT) is a synthetic biodegradable polymer with high flexibility and a high potential for functionalization, aiming at bactericidal, antimicrobial, or antifungal properties. In this work, the casting method was used to prepare PBAT films containing *Moringa oleifera* (MO) seed powder. The MO was added in different contents of 0, 1, 3, 5, and 10% (wt) to functionalize the film properties and its efficiency as strawberry packaging. The PBAT films containing 1% (wt) of MO were the most suitable for packaging applications, considering the mechanical properties and thermal properties. MO did not present significant interactions with the PBAT matrix and reduced the PBAT crystallinity, leading to a decrease in gas and water vapor permeabilities. The PBAT-1% MO films showed good performance as biodegradable packaging for strawberry storage, prolonging their storage time and reducing their vulnerability to fungal attack. Besides, the MO decreased the fungal contamination of strawberries when compared to those stored in neat PBAT. The developed films performance suggests that the PBAT/MO films have good potential to be used as active food packaging.

**Keywords** Packaging · *Moringa oleifera* · Strawberry · Active films · PBAT

## Introduction

Packaging plays a fundamental role in the storage, transportation, and maintenance of food quality. Fresh foods, such as fruits and vegetables, are known for their short shelf life, resulting in high losses in relatively short times (~ 10 days) [1]. Among the primary packaging used by the food industry, commodity polymers are mainly used, with a production of 360 million tons worldwide every year [2]. The basic

polymers used for packaging are polyethylene, polypropylene, polyvinyl chloride, polystyrene, and polyethylene terephthalate. Despite being low-density and low-cost materials, these polymers present significant ecological issues for their disposal due to their high degradation time [3]. As an alternative to the top plastic generation with environmental problems in the packaging sector, biodegradable polymers have proven to be good alternatives in replacing the materials currently used [4, 5].

Biodegradable polymers have been studied as food packaging and coatings, as they have good mechanical and thermal properties and are non-toxic. As viable choices to produce the films, poly(butylene adipate-*co*-terephthalate) (PBAT) is a synthetic biodegradable polymer with high flexibility and a high potential for application in food packaging, as cited in the literature [6]. Due to differences in chemical structure, crystallinity, and barrier properties, in general, biodegradable films are functionalized, aiming to add function and improve performance [7, 8].

Several active agents are added among active or functional packaging materials, aiming at bactericidal, antimicrobial, or antifungal properties [1]. Among the primary

**Electronic supplementary material** The online version of this article (<https://doi.org/10.1007/s13726-020-00885-7>) contains supplementary material, which is available to authorized users.

✉ Derval dos Santos Rosa  
dervalrosa@yahoo.com.br; derval.rosa@ufabc.edu.br

<sup>1</sup> Centro de Engenharia, Modelagem e Ciências Sociais Aplicadas-CECS/Universidade Federal Do ABC (UFABC)- Santo André, Avenida Dos Estados, 5001, Santo André, SP 09210-580, Brazil

<sup>2</sup> Packaging Technology Center-Instituto de Tecnologia de Alimentos-Cetea/Ital-Campinas, Avenida Brasil 2880, Campinas, SP 13070-178, Brazil

materials used, TiO<sub>2</sub>, Ag, and Au nanoparticles are the main antimicrobial agents. However, various natural fibers have been used to prepare PBAT compounds, such as manga wastes, essential oregano oil, and natural fibers from the Amazon rainforest [9–11]. *Moringa oleifera* seed powder has stood out in recent years [12–14]. This material contains high-quality protein (~52%) and essential amino acids, which confers antimicrobial properties. Also, the seeds are rich in oils and glycosylates [14, 15]. The bactericidal effects of these proteins, contained in the powder, were confirmed for several microorganisms [16–19].

In this work, the PBAT/*M. oleifera* (MO) seed powder composites with different MO contents were prepared by film extension (casting) method for application in food packing for strawberry. Morphology, chemical composition, thermal stability, and crystallinity evaluated the MO properties. Various techniques characterized the films, including mechanical tests, SEM, FT-Raman, TGA, DSC, XRD, oxygen and water vapor permeability, and their strawberry application performance. The overarching aims of this research were twofold: (i) examine the effect of MO content on PBAT/*Moringa* composites, and (ii) to evaluate the performance of the developed composites as food packaging.

## Experimental

### Materials

Poly (butylene adipate-*co*-terephthalate) (PBAT) ( $M_w$  66,500 g/mol) was purchased from BASF (São Paulo, Brazil) under the trade name Ecoflex. *M. oleifera* seeds were purchased from a local producer (Casa Nova-Bahia, Brazil). Chloroform (1.48 g/cm<sup>3</sup> density at 25 °C) was purchased from Synth (Diadema-SP, Brazil).

### Preparation of *M. oleifera* powder

The seeds were dried for 24 h at 60 °C. The dried seeds were peeled and reduced to powder using a home-made processor (Mondial Power 21,500 W) for 10 min. A magnetic sieve separated the resulting powder for 10 min, and the opening, selected for separation of the powder size, was mesh #200 (75 μm). The sample was named MO.

### Preparation of composite films by extension method

PBAT was first dried at 50 °C for 24 h before use. Then, 20 g of PBAT was dissolved in 100 mL of chloroform with constant magnetic stirring. The polymeric solution was then applied to a glass plate (13 × 18 cm) and extended in film form using a wire extender TKB Erichsen (200 μm). The

plates were air-dried for 1 min, in order to partial evaporation of the solvent (flash-off). The plates were then immersed in demineralized water, in polyethylene trays of 24 × 32 cm (internal dimensions) to perform a coagulation bath. Films were detached from the glass plate's surface (peel-off effect) and removed from the solution to dry. For composites, MO powder was incorporated after the solubilization of PBAT in different contents of 1, 3, 5, and 10% (wt). Figure 1 shows the methodology schematically.

## Characterization

### Optical microscopy and scanning electron microscopy

The MO power was evaluated by optical microscopy (ZEISS microscope, model AXIO Scope A1), with 50-fold magnification. A granulometric analysis measured the particles' sizes. An MEV FEI Quanta 250 scanning electron microscope examined the *Moringa* powder's morphological characteristics and the developed films. The samples were previously covered with gold by the sputtering technique (Leica ACE200) with a 20 nm gold deposition on the samples' surface.

### Fourier transform infrared spectroscopy (FTIR)

An equipment Frontier 94,942 (PerkinElmer, USA) collected the FTIR data, in the range of 400–4000 cm<sup>-1</sup>, with 64 scans and a 4 cm<sup>-1</sup> resolution, equipped with an attenuated total reflectance (ATR) accessory with diamond. Origin 8 software processed the data.

### Fourier transform Raman spectroscopy (FT-Raman)

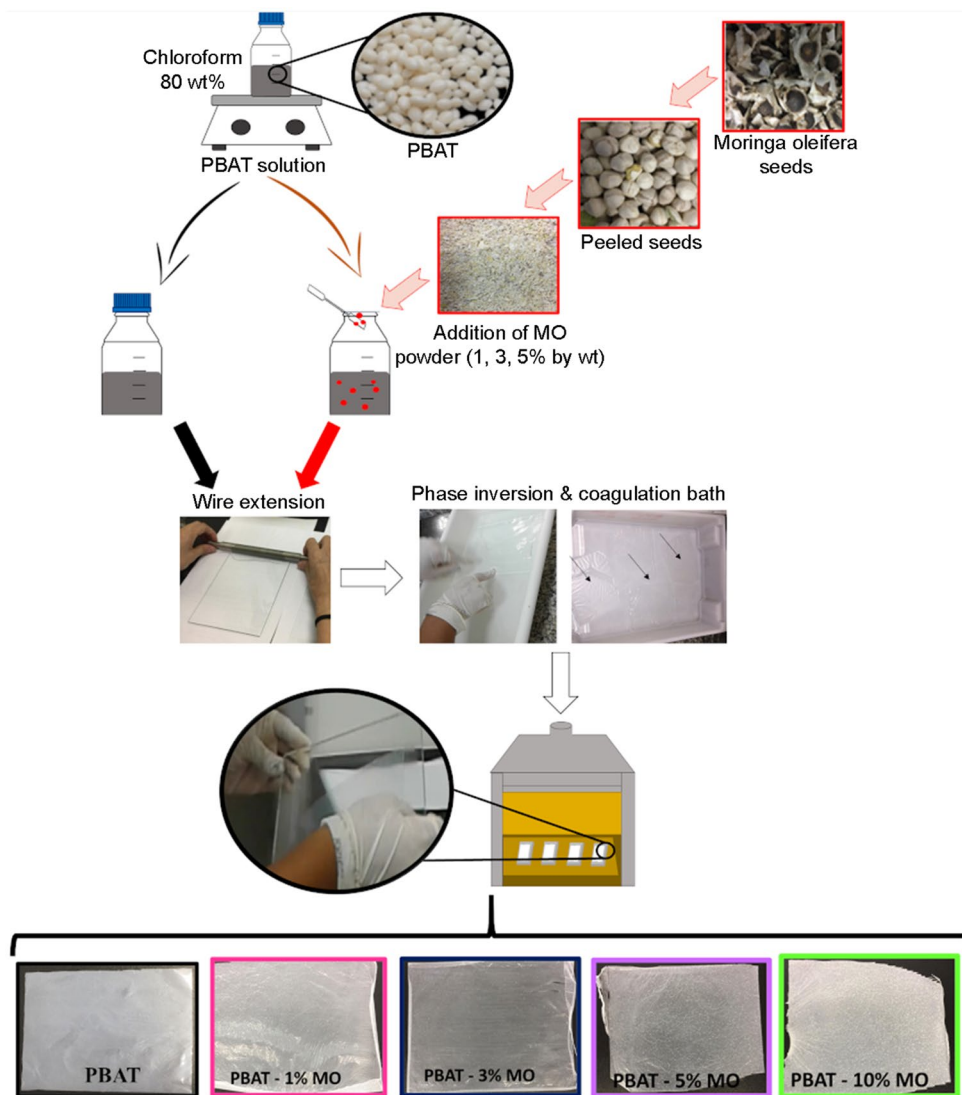
The samples were analyzed using an FT-Raman equipment (MultiRaman, Bruker Optics) equipped with a 1064 nm wavelength and a 150 W power laser. The data acquisition parameters were: 600–4000 cm<sup>-1</sup>, 32 scans, and 4 cm<sup>-1</sup> spectral resolution.

### X-ray diffraction (XRD)

A D8 Focus diffractometer (Bruker AXS-Karlsruhe, Germany) collected the data using monochromatic CuK<sub>α</sub>1 radiation  $\lambda = 1.54056 \text{ \AA}$ , operating at 40 kV and 40 mA, with a step width of 0.015° and counting time of 100 s at each 0.5°, from 2θ of 10°–50°. The crystallinity index was calculated by Eq. (1) [20]:

$$CI = \frac{(I_{200} - I_{am})}{I_{200}} \quad (1)$$

**Fig. 1** Flow diagram representative of the PBAT composites preparation



$I_{200}$  is the peak of highest intensity ( $2\theta \sim 22.5$ ), and  $I_{am}$  is the peak lowest intensity ( $2\theta \sim 18$ ).

### Thermogravimetric analysis (TGA)

The thermogravimetric analysis was conducted on an STA 6000 equipment (PerkinElmer, USA), using alumina pans. The samples were heated from 30 to 600 °C at a rate of 10 °C/min under nitrogen atmosphere with a flow rate of 20 mL/min.

### Mechanical tests

The tensile tests were investigated by an equipment Instron 3367 (Norwood, USA) at room temperature by the standard ASTM D638-14, with a load cell of 50 N and a test speed of 50 mm/min. The compositions were tested in quintuplicate.

### Differential scanning calorimetry (DSC)

A DSC Q-series (TA Instruments) (New Castle, Delaware, USA) collected the DSC data under the nitrogen atmosphere (50 mm/min). The samples were heated to 190 °C, cooled to – 60 °C and, then heated to 200 °C. Equation (2) describes the calculation of the degree of crystallinity ( $X_c$ ), where  $\Delta H_m$  is the experimental fusion enthalpy, and  $\Delta H_{100\%}$  is the theoretical enthalpy of PBAT (114 J/g).

$$X_c(\%) = \frac{\Delta H_m}{\Delta H_{100\%}} \times 100 \quad (2)$$

## Oxygen and water vapor permeability

The oxygen transmission rate ( $O_2TR$ ) was determined according to the ASTM D 3985-17 at  $23 \pm 0.5$  °C in a coulometric sensor equipment (Mocon, Oxtran model ST, IL, USA). The film outer side was placed in contact with the permanent gas (100%  $O_2$ ). The readings were corrected to 1 atm of partial pressure gradient of permanent gas and oxygen partial pressure gradient between the two surfaces of film. This gradient corresponds to the driving force for oxygen permeation through the film.

Once  $O_2TR$  was determined, the oxygen permeability coefficient was calculated by Eq. (3):

$$O_2P = \frac{O_2TR \cdot L}{P(1)} \quad (3)$$

where,  $O_2P$  is the oxygen permeability coefficient ( $mL$  (CNTP)  $mm^{-2} day^{-1} atm^{-1}$ ),  $O_2TR$  is the oxygen transmission rate ( $mL$  (CNTP)  $m^{-2} day^{-1}$ ),  $L$  is the mean film thickness ( $\mu m$ ), and  $P$  is the oxygen partial pressure in the gas chamber permeating the diffusion cell (1 atm). The partial pressure of  $O_2$  in the carrier gas chamber ( $N_2 + H_2$ ) is considered null.

The water vapor transmission rate (WVTR) followed the ASTM E 96/E 96M-05 methods at  $25 \pm 0.5$  °C, and anhydrous calcium chloride (0% RH) filled the cells. The cells were covered with the films, sealed, and placed in a climatic chamber (Votsch, VC 0063 model, German) at  $75 \pm 2\%$  RH. Once the WVTR was determined, Eq. (4) determined the water vapor permeability coefficient.

$$WVP = \frac{WVTR \cdot L}{PWVS(RH1 - RH2)} \quad (4)$$

where, WVP is the water vapor permeability coefficient ( $g$  water  $mm^{-2} day^{-1} mmHg^{-1}$ ), WVTR is the water vapor transmission rate through a film ( $g$  water  $m^{-2} day^{-1}$ ),  $L$  is the mean film thickness ( $\mu m$ ), PWVS is the partial water vapor saturation pressure at the test temperature ( $mmHg$ ). RH1 is the chamber relative humidity (0.75), and RH2 is the relative humidity inside the capsule with desiccant (0% RH).

## Films performance as packaging for strawberries

Strawberries were purchased from a local farm (Santo André-SP, Brazil) and immediately treated with sodium hypochlorite (250 ppm), and then dried at room temperature. Fruits of uniform size and free of fungal actions or physical damage were selected. The washed fruits were put in PBAT films and their composites and sealed by a manual plastic packaging sealer at a temperature of 120 °C (TECNAL STN, São Paulo, Brazil). Low density polyethylene (LDPE)

and polyvinyl chloride (PVC) films were used to compare commercial materials with the new formulation [21, 22]. A refrigerator at 4 °C stored the samples. Photographs were taken from the fruits at the beginning of the experiment, and after 3, 7, 10, and 15 days of storage [23].

## Results and discussion

### *M. oleifera* seed powder characterization

#### Granulometry and morphological analysis

The optical microscopy evaluated the morphology and regularity of the power, as shown in Fig. 2a. The particles were analyzed by the Image J software to measure the particle diameter, and the average diameter was  $40.9 \pm 9.7$   $\mu m$ . Figures 2b, c show the scanning electron micrographs of MO power. This material is heterogeneous and has a relatively porous matrix [24]. This porosity, according to Shirani et al. contributes to the efficiency of this biopolymer in removing bacteria and fungi [25].

#### FTIR and FT-Raman

Infrared spectroscopy investigated the MO powder structure in the dried state. The typical spectrum (Fig. 1S, Supplementary Material) showed peaks between 4000 and 1000  $cm^{-1}$ . The peak in the region of 3500–3200  $cm^{-1}$  indicates alcohol or phenol, a functional group predominant in the structures of proteins and fatty acids present in *M. oleifera* seeds [26]. The peak below 3400  $cm^{-1}$  indicates NH elongation, and intense peaks at 3398  $cm^{-1}$  are associated with –OH elongation [27]. Bands between 2800 and 2900  $cm^{-1}$  are associated with the extent of CH vibration, and their high intensity is also associated with the presence of long carbon chain compounds, that is, the methylene groups in lipid and cellulose molecules [28]. The presence of bands between 1800  $cm^{-1}$  and 1500  $cm^{-1}$ , observed in Fig. 2d, is related to proteins and amino acids. The peak at 1748  $cm^{-1}$  represents carboxylic groups. The band between 1669 and 1527  $cm^{-1}$  provides the stretching vibration added to the carbonyl group (C=O) [29].

*M. oleifera* active groups are mainly proteins. Under suitable conditions, these proteins can be extracted from the seed to obtain a concentrated extract, or they can also be obtained from the seed in nature through the exudation process, which occurs naturally. According to Kwaambwa and Maikokera, the organic groups of MO protein are characteristic of amide I and II [30]. The spectra showed two strong absorption bands of 1658 and 1544  $cm^{-1}$  of amides I (protein  $\alpha$ -coil helix) and II, respectively, which

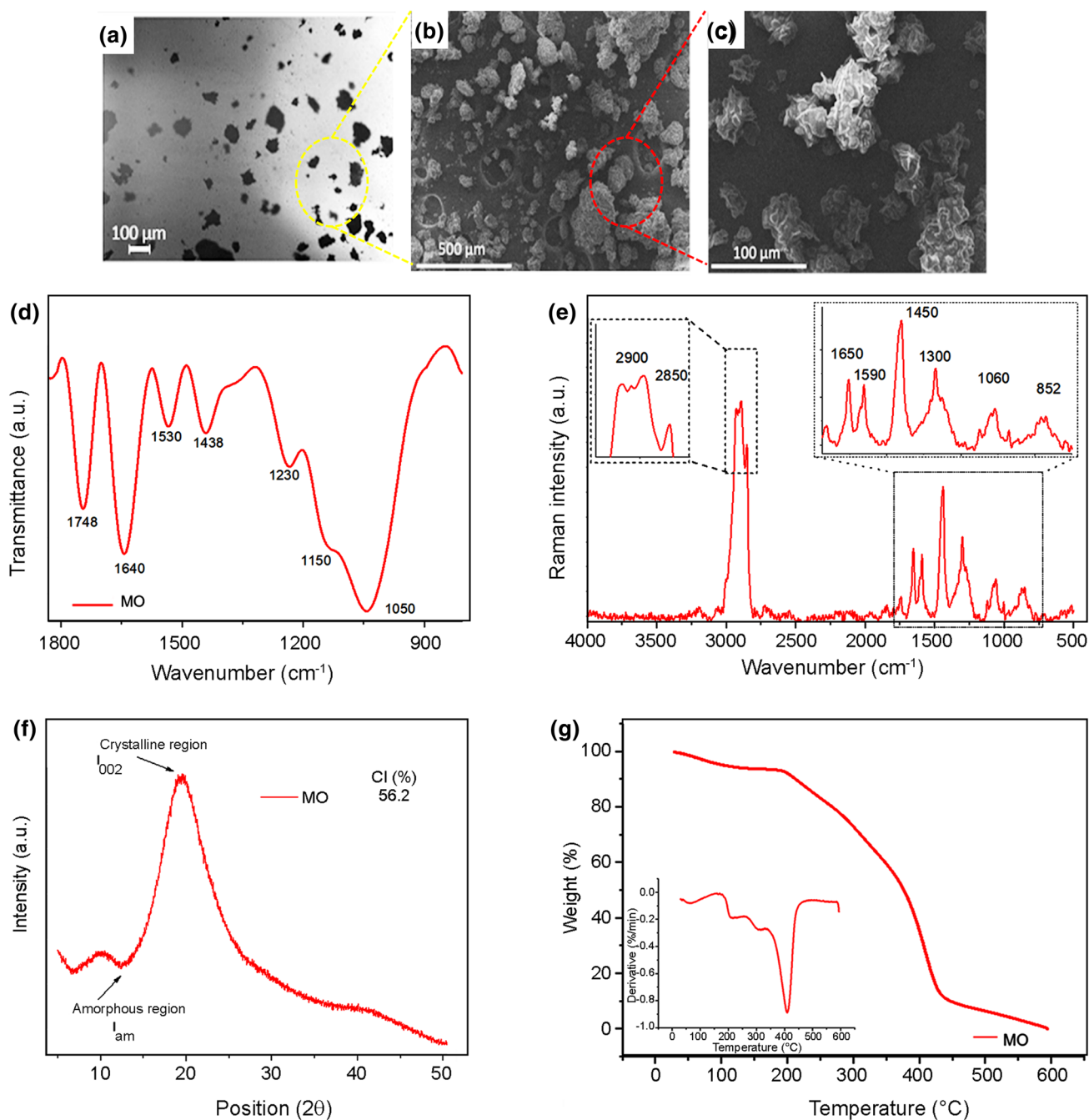


**Fig. 2** **a** Optical microscopy image of the *Moringa oleifera* seed powder. **b, c** Scanning electron microscopy with different zooms of the MO sample. **d** FTIR spectrum zoom between 1800 and 800  $\text{cm}^{-1}$ . **e**

FT-Raman spectrum of MO with inserts from the 2950–2800  $\text{cm}^{-1}$  and 1700–800  $\text{cm}^{-1}$  regions. **f** XRD. **g** TGA of *M. oleifera* powder

confirmed the structure of the protein present in the *Moringa* seeds [31, 32].

Flexion vibrations between 1449 and 1338  $\text{cm}^{-1}$  represented O–H and C–N (from aromatic amines) [29]. The peaks at 1230, 1150, and 1050  $\text{cm}^{-1}$  represented acetyl groups present in the lignin structure, and C–O and C=O

elongation of ether, ester, and phenol bonds, respectively [33].

Raman spectroscopy was used as a complementary technique to FTIR to analyze the structure and functional groups of the ground *Moringa* seed (Fig. 2e). The peaks 2930, 2910, and 2850  $\text{cm}^{-1}$  were assigned to =CH<sub>2</sub> stretch. The peaks



of 1650 and 1590  $\text{cm}^{-1}$  corresponded to amide groups I and II, respectively [34]. The peaks at 1450 and 1300  $\text{cm}^{-1}$  were associated with C–NH vibrations of tertiary amides [35], while at 1060 and 852  $\text{cm}^{-1}$  they were associated with C–C=CH<sub>2</sub> stretches and the CCO– vibration, respectively.

### X-ray diffraction (XRD)

Figure 2f shows the diffractograms of MO powder. The seeds are composed of a high amount of oil, protein, and a cellulose fraction. The characteristic XRD peak at 22.5° is associated with the plane (002), and the amorphous region was verified at 12.5° [34]. Segal equation analyzed the crystallinity index (CI), and a CI value of 56% was obtained, which corroborates the literature [28].

### Thermogravimetric analysis (TGA)

Figure 2g shows the MO thermogram. The sample has three main events of weight loss: the first occurs between 30 and 130 °C and is associated with loss of water, volatiles, and low molar mass components. The second is associated with the loss of gases, such as CO<sub>2</sub> and NH<sub>3</sub>, resulting from the protein amine groups [34]. The third event occurs from 300 to 428 °C, which corresponds to the MO powder [36, 37].

### Films characterization

#### Mechanical tests

Mechanical properties are essential for food packaging since good flexibility and mechanical resistance are required to protect the food during handling, transport, and storage. Table 1 shows the mechanical properties of films. The PBAT showed stiffness values of approximately 160 MPa and  $\epsilon$  of ~125%; these values are consistent with those reported in the literature [38, 39]. The MO addition decreased the  $E$ ,  $\sigma$ , and  $\epsilon$  associated with the weak stress transformation across interphase [40]. However, there is another possibility to explain the mechanical resistance: the composite's

**Table 1** Results of the tensile test of films containing Moringa powder: elastic modulus ( $E$ ), tensile strength ( $\sigma$ ), and elongation-at-break ( $\epsilon$ )

Samples	Elastic modulus ( $E$ ) (MPa)	Tensile strength ( $\sigma$ ) (MPa)	Elongation-at-break ( $\epsilon$ ) (%)
PBAT	161.7 ± 28.1	7.7 ± 0.8	124.6 ± 23.7
PBAT-1% MO	84.2 ± 2.8	3.8 ± 1.9	78.6 ± 19.2
PBAT-3% MO	44.6 ± 3.4	1.5 ± 0.2	74.4 ± 5.8
PBAT-5% MO	43.7 ± 4.4	1.3 ± 0.5	50.7 ± 9.1
PBAT-10% MO	56.7 ± 5.9	1.3 ± 0.4	30.8 ± 7.0

preparation method. During the phase inversion process, the polymer was submerged in water, which induced the formation of pores in the films due to MO's high hydrophilicity, reducing the final material [39, 41, 42].

According to conventional standards,  $\sigma$  for packaging film must be > 3.5 MPa [43]. Thus, PBAT-1% MO is most suitable for such an application. The other compositions showed a significant decrease in mechanical properties, associated with MO's high content, leading to possible pores appearance.

### Scanning electron microscopy

SEM images reveal information about the morphology of composites and filler dispersion. The neat PBAT showed a smooth and homogeneous surface, as presented in Fig. 3a. After the addition of MO, a porous and highly rough surface was formed. The indicative arrows in the photomicrographs indicate voids formed by the absence of a reinforcement phase. According to Moustafa et al. this behavior can indicate *M. oleifera* particles [44]. Despite the matrix being porous, Wu et al. stated that variations in oxygen or water vapor permeation occur in active packaging and positively influence food storage [45].

### Thermal properties

Figure 3b shows the TGA curves and their derivative thermogravimetric (DTG) curves of all the composites. PBAT showed a  $T_{10\%}$  of 377.7 °C and  $T_{\text{max}}$  of 402.6 °C, with a single weight-loss event. The values found are similar to those reported in literature [46]. The PBAT thermal degradation is associated with the C–C bonds cleavage present in the polymer structure [47]. After the addition of MO, no separate degradation stage occurred, which indicates that *M. oleifera* has been entirely covered by PBAT molecules [48].

Table 2 summarizes the DSC results, and Fig. 2S (Supplementary Material) shows the second heating and cooling curves. The PBAT-MO samples have higher  $T_g$  values, and PBAT-1% MO presents the high values attributed to the uniform dispersion of MO, and probably this sample shows the best adhesion/cover between PBAT and MO [13]. The *M. oleifera* restricts the mobility of polymer segments and increases the glass transition temperatures. No significant differences were observed in the melting temperature [11].

The  $T_c$  values significantly increased after the MO addition, which means that the MO facilitates PBAT crystallization, acting as a nucleating agent [49]. The slight changes observed in the  $X_c$  values are associated with a possible change in polymer crystallization kinetics. Smaller amounts of MO do not affect crystallization, while larger amounts limit the crystallite growth, generating a smaller size crystalline phase, reflecting the decrease in  $X_c$  values.

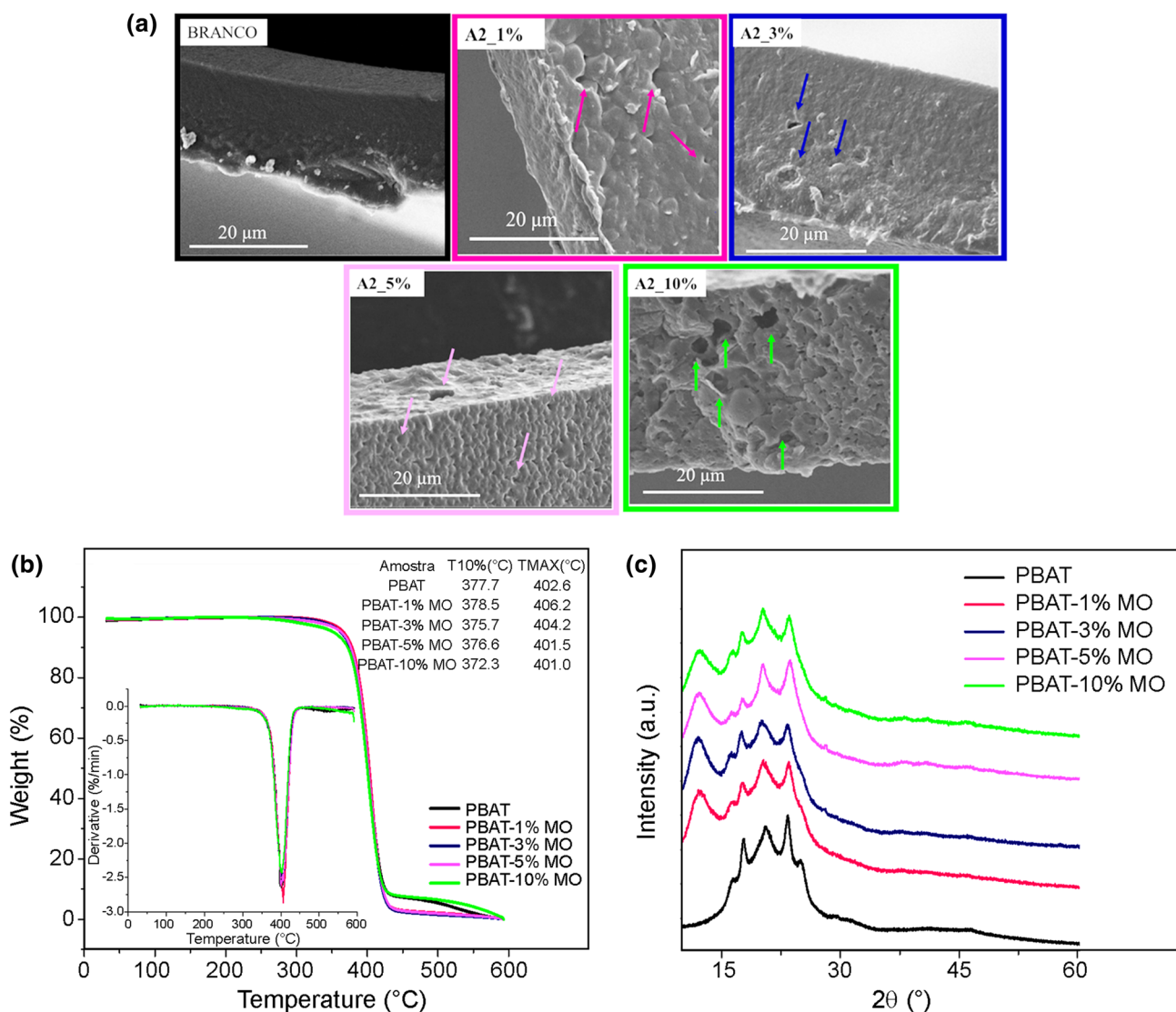


**Fig. 3** a SEM micrographs of the fractured surfaces for neat PBAT and its composites, and the arrows indicate the voids presence. b TGA and DTG curves of the neat PBAT and its composites. c X-ray diffraction patterns of the PBAT and PBAT-MO

**Table 2** DSC results of PBAT and PBAT-MO samples ( $T_g$ ,  $T_m$ ,  $\Delta H_m$ ,  $T_c$ ,  $X_c$ ), and crystallinity index (CI) calculated from XRD results; oxygen permeability coefficient ( $O_2P$ ) and water vapor permeability coefficient (WVP) of PBAT films without and with *M. oleifera*

Sample	$T_g$ (°C)	$T_m$ (°C)	$\Delta H_m$ (J/g)	$T_c$ (°C)	$X_c$ (%)
PBAT	- 43.2	124.2	11.5	68.7	10.1
PBAT-1% MO	- 34.8	125.5	13.1	78.1	11.5
PBAT-3% MO	- 35.7	124.5	10.9	76.2	9.5
PBAT-5% MO	- 36.1	124.8	10.1	78.8	8.8
PBAT-10% MO	- 39.8	122.8	8.6	79.3	7.5

Sample	$O_2P$ [mL (STP) $\mu\text{m}^{-2} \text{day}^{-1} \text{atm}^{-1}$ ]	WVP (g water $\mu\text{m}^{-2} \text{day}^{-1} \text{mmHg}^{-1}$ )
PBAT	31.1 ± 1.0	323.3 ± 26.6
PBAT-1% MO	62.9 ± 9.5	382.8 ± 9.1
PBAT-3% MO	102.3 ± 0.6	455.9 ± 4.7
PBAT-5% MO	199.8 ± 5.1	692.9 ± 24.1
PBAT-10% MO	719.5 ± 2.6	774.5 ± 13.6

**Table 3** Crystallinity index (CI) obtained from XRD patterns

Sample	Crystallinity index (%)
PBAT	9.7
PBAT-1% MO	8.2
PBAT-3% MO	9.6
PBAT-5% MO	8.5
PBAT-10% MO	7.6

### X-ray diffraction

XRD was used to examine the crystallinity of PBAT and the PBAT/MO samples (Fig. 3c). PBAT exhibits five characteristic diffraction peaks at 16.2°, 17.3°, 20.4°, 23.4°, and 25.2°, associated with the planes (011), (010), (110), (100), and (111) [50, 51]. The PBAT diffraction pattern remained unchanged after the MO addition. No transcrystalline phases were created in the system interface [50]. Small shifts were observed for the PBAT structure, emphasizing the 20.4° angle, which shifted to ~20.0°. This small variation may indicate a change in the formation of PBAT crystallites. However, a new broad peak at 12° was detected, which can be associated to the MO XRD pattern, confirming MO incorporation in the composites. Table 3 shows the crystallinity values obtained by XRD patterns.

The crystallinity differences observed between the XRD and the DSC can be associated with the test methodology. While the DSC occurs through the polymer melting and cooling, the XRD is performed on the prepared films. Since in the present study, the films were prepared by wire extension, the XRD data is closer to the real crystalline structure found in the developed films.

### Oxygen permeability and water vapor permeability

The addition of MO (Table 2) greatly influenced the O<sub>2</sub>P and WVP values. PBAT is a polymer with high O<sub>2</sub>P and WVP values due to its chemical structure and physical properties, such as low crystallinity [52, 53]. The addition of *M. oleifera* decreased the films oxygen barrier properties, which can be attributed to the films lower crystallinity, i.e., the MO reduced the films abilities to act as oxygen barriers [54]. The oxygen permeabilities increased rapidly with the powder Moringa content when the latter is over 3% (wt), resulting in blend films with weaker oxygen barrier properties [55]. The O<sub>2</sub>P is highly dependent on film structure, thickness, void volume, and arrangement of the polymer chain [56]. As previously described, the addition of Moringa resulted in low interactions between the PBAT matrix and the MO powder. Thus, the presence of pores changed the PBAT chain arrangement. Despite the increase in O<sub>2</sub>P values, it is important to note that the Moringa seed has

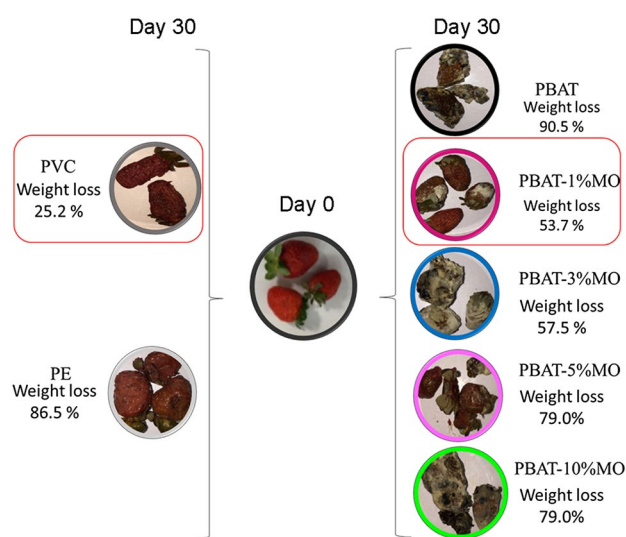
known active properties. Thus, with the balance between the OM functionality and the permeability, the developed packaging, mainly the films PBAT-1% MO, is suitable for certain foods, such as strawberries.

Table 2 also shows the WVP values of PBAT films without and with MO. The addition of MO powder increased the WVP values, which the interaction between PBAT and powder Moringa can decrease the water vapor barrier properties. The MO is a hydrophilic material that favors transfer of water molecules through the film [57]. Besides, the lower crystallinity of film favors the diffusion of water molecules since the polymer chains are less densely packed due to *M. oleifera* powder. The PBAT and PBAT-1% MO films showed very similar water vapor permeability coefficients. Furthermore, increasing the powder content increases the WVPs of the films [55].

### Films performance as packaging for strawberries

The strawberries are highly susceptible to rapid loss of water owing to respiration and transpiration. Commonly, weight loss occurs during the fruit storage because of its respiratory process, humidity transfer, and oxidation [58]. Figure 4 shows strawberries before packaging after the last test day (day 30). In Fig. 4, it is also possible to observe mass loss suffered by the fruits after 30 days. Figure 3S (Supplementary Material) shows the packaged strawberries and the visual changes observed after 0, 3, 7, 10, and 15 days.

The weight loss harms appearance of strawberry fruits, leading to shrinkage and opaque-looking skin. Fruit storage is an important parameter that controls and slows deterioration [59].

**Fig. 4** Digital images of the appearance of strawberries at days 0 and 30



The samples that showed less weight loss were PVC (25.2%) and PBAT-1% MO (53.7%). According to the literature, PVC film used as a control sample has low permeability rates to oxygen and water vapor, which justifies its small mass loss and the absence of fungi visible to the naked eye. Besides, the strawberry did not lose the water, which maintained its weight [60].

Considering the PBAT samples without and with MO, neat PBAT was the one that presented the most significant loss of fruit mass after 30 days of storage. Also, films with 3, 5, and 10% MO showed the highest amounts of visible fungi, while the sample with 1% MO was the one with the least damaged and contaminated strawberries. It can be associated with the agglomeration effect: while 1% showed good dispersion, the other contents may have resulted near of the particles to each other, which limited the release of the active agent. The presence of MO in small amounts can cause cell damage in mold and yeast, altering the synthesis

of fungal enzymes [61, 62]. Thus, morphological changes can occur and cause structural changes and molecular disorganization in fungal cells [63] (Fig. 5). As observed in the FTIR analysis, the seeds have distinct groups that show protein in the MO powder. Exudation of Moringa proteins (i.e., active compound) from the powder surface to the films results in damage to microbial cell membranes, minimizing the fungal attack on strawberries.

The biodegradable films effectively delay senescence, making the fruits more vulnerable to pathogenic infection due to loss of cellular or tissue integrity. Therefore, PBAT-1% MO films were useful as biodegradable packaging for storing sensitive fruits, such as strawberries, by prolonging their storage time and reducing their vulnerability to fungal attack. The packaging is biodegradable and is a potential substitute for the commodities currently used, and its performance is comparable to the performance of PE packaging.

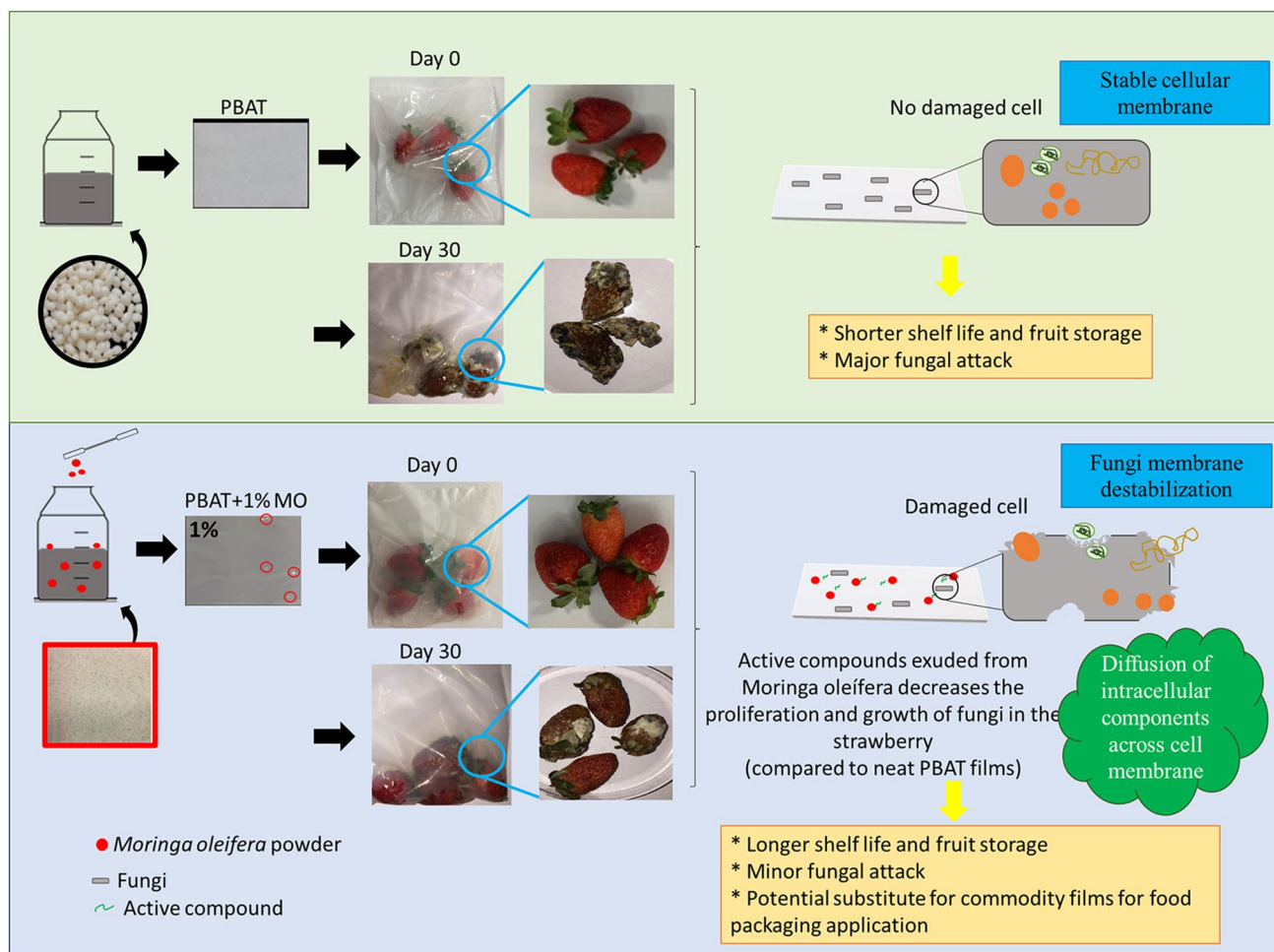


Fig. 5 Schematic representation of the addition of MO in PBAT films and its effect on the strawberry’s storage

## Conclusion

PBAT/MO films were successfully prepared using *M. oleifera* (MO) seeds in the powder form. Samples containing 1% MO showed the best results in their mechanical properties. The maximum stress values correspond to the values of international standards required for packaging applications (above 3.5 MPa). The films showed good thermal stability, only slightly decreased for samples with higher MO content. The PBAT/MO samples showed higher  $T_g$  values since the MO particles restricted mobility of polymer segments. No changes were observed on  $T_m$  values associated with the absence of chemical interaction between the MO and the PBAT. These results were confirmed by FT-Raman analysis. However, the absence of interactions can be beneficial, considering MO available active sites for subsequent interaction with pathogenic microorganisms. The reinforcement addition reduced the crystallinity of the films, changing the structural organization of PBAT polymer chains. The lower crystallinity reflected in the oxygen and water vapor permeability and the films containing *M. oleifera* showed high permeability, which increased with MO content. Possibly, due to permeability changes, the films containing MO allowed the strawberries to breathe more efficiently, which delayed their deterioration. Only the 1% MO sample showed consistent results for use in packaging. PBAT-1% MO films showed good performance as packaging for strawberry storage, prolonging their storage time, and reducing their vulnerability to fungal attack.

**Acknowledgements** The authors thank the financial support provided by CNPQ (305819/2017-8) and FAPESP (2018/11277-7), CNPq, CAPES (Code 001), Revalores Strategic Unit, and the Multiuser Experimental Center of the Federal University of ABC (CEM-UFABC).

## Compliance with ethical standards

**Conflict of interest** The authors declare that there are no conflicts of interest.

**Availability of data and material** The authors are willing to provide the manuscript's data, if necessary.

**Code availability** Not applicable.

## References

1. Abrial H, Arikisa J, Mahardika M, Handayani D, Aminah I, Sandrawati N (2020) Transparent and antimicrobial cellulose film from ginger nanofiber. *Food Hydrocoll* 98:105266
2. Facts P (2019) An analysis of European plastics production, demand and waste data. [https://www.plasticseurope.org/application/files/9715/7129/9584/FINAL\\_web\\_version\\_Plastics\\_the\\_facts\\_2019\\_14102019.pdf](https://www.plasticseurope.org/application/files/9715/7129/9584/FINAL_web_version_Plastics_the_facts_2019_14102019.pdf)
3. Akshaykranth A, Rao TV, Kumar RR (2020) Growth of ZnO nanorods on biodegradable poly (lactic acid) (PLA) substrates by low temperature solution method. *Mater Lett* 259:126807
4. Ilyas RA, Sapuan SM, Sanyang ML, Ishak MR, Zainudin ES (2018) Nanocrystalline cellulose as reinforcement for polymeric matrix nanocomposites and its potential applications: a review. *Curr Anal Chem* 14:203–225
5. Mangaraj S, Yadav A, Bal LM, Dash SK, Mahanti NK (2019) Application of biodegradable polymers in food packaging industry: a comprehensive review. *J Packag Technol Res* 3:77–96
6. Saibuatrong W, Cheroennet N, Suwanmanee U (2017) Life cycle assessment focusing on the waste management of conventional and bio-based garbage bags. *J Clean Prod* 158:319–334
7. Hasheminejad K, Montazeri A (2020) Enhanced interfacial characteristics in PLA/graphene composites through numerically-designed interface treatment. *Appl Surf Sci* 502:144150
8. Chiarathanakrit C, Riyajan SA, Kaewtatip K (2018) Transforming fish scale waste into an efficient filler for starch foam. *Carbohydr Polym* 188:48–53
9. Nawab A, Alam F, Hasnain A (2017) Mango kernel starch as a novel edible coating for enhancing shelf- life of tomato (*Solanum lycopersicum*) fruit. *Int J Biol Macromol* 103:581–586
10. Cardoso LG, Santos JC, Camilloto GP, Miranda AL, Druzian JI, Guimarães AG (2017) Development of active films poly (butylene adipate-co-terephthalate)-PBAT incorporated with oregano essential oil and application in fish fillet preservation. *Ind Crops Prod* 108:388–397
11. Ferreira FV, Pinheiro IF, Mariano M, Cividanes LS, Costa JC, Nascimento NR, Kimura SP, Neto JC, Lona LM (2019) Environmentally friendly polymer composites based on PBAT reinforced with natural fibers from the amazon forest. *Polym Compos* 40:3351–3360
12. Takassugui KS, Arantes CC, de Jesus TA (2019) Comparação da remoção de turbidez e cor aparente em filtros lentos de areia com e sem adição de proteína imobilizada de *Moringa oleifera*. *Rev Bras Ciência Tecnol e Inovação* 4:169
13. de Nunes EC, de Souza AG, dos Rosa DS (2019) Use of a chain extender as a dispersing agent of the CaCO<sub>3</sub> into PBAT matrix. *J Compos Mater* 54:1373–1382
14. Jain A, Subramanian R, Manohar B, Radha C (2019) Preparation, characterization and functional properties of *Moringa oleifera* seed protein isolate. *J Food Sci Technol* 56:2093–2104
15. Chen R, Wang XJ, Zhang YY, Xing Y, Yang L, Ni H, Li HH (2019) Simultaneous extraction and separation of oil, proteins, and glucosinolates from *Moringa oleifera* seeds. *Food Chem* 300:125162
16. Landázuri AC, Villarreal JS, Núñez ER, Pico MM, Lagos AS, Caviedes M, Espinosa E (2018) Experimental evaluation of crushed *Moringa oleifera* Lam. seeds and powder waste during coagulation–flocculation processes. *J Environ Chem Eng* 6:5443–5451
17. Fernandes DM, Sousa RM, de Oliveira A, Morais SA, Richter EM, Muñoz RA (2015) *Moringa oleifera*: a potential source for production of biodiesel and antioxidant additives. *Fuel* 146:75–80
18. Gopalakrishnan L, Doriya K, Kumar DS (2016) *Moringa oleifera*: a review on nutritive importance and its medicinal application. *Food Sci Hum Wellness* 5:49–56
19. Dezfooli SM, Uversky VN, Saleem M, Baharudin FS, Hitam SM, Bachmann RT (2016) A simplified method for the purification of an intrinsically disordered coagulant protein from defatted *Moringa oleifera* seeds. *Process Biochem* 51:1085–1091
20. Segal L, Creely JJ, Martin AE, Conrad CM (1959) An empirical method for estimating the degree of crystallinity of native cellulose using the X-ray diffractometer. *Text Res J* 29:786–794
21. Ritchie DA (2012) Ampere using single electron pumps. *Nat Commun* 3:930–936

22. Mali S, Grossmann MVE (2003) Effects of yam starch films on storability and quality of fresh strawberries (*Fragaria ananassa*). *J Agric Food Chem* 51:7005–7011
23. Garcia PS, Grossmann MV, Shirai MA, Lazaretti MM, Yamashita F, Muller CM, Mali S (2014) Improving action of citric acid as compatibiliser in starch/polyester blown films. *Ind Crops Prod* 52:305–312
24. Araújo CS, Alves VN, Rezende HC, Almeida IL, De Assuncao R, Tarley CR, Segatelli MG, Coelho NM (2010) Characterization and use of *Moringa oleifera* seeds as biosorbent for removing metal ions from aqueous effluents. *Water Sci Technol* 62:2198–2203
25. Shirani Z, Santhosh C, Iqbal J, Bhatnagar A (2018) Waste *Moringa oleifera* seed pods as green sorbent for efficient removal of toxic aquatic pollutants. *J Environ Manage* 227:95–106
26. Matinise N, Fuku XG, Kaviyarasu K, Mayedwa N, Maaza M (2017) ZnO nanoparticles via *Moringa oleifera* green synthesis: physical properties and mechanism of formation. *Appl Surf Sci* 406:339–347
27. Saran M, Vyas S, Mathur M, Bagaria A (2018) Green synthesis and characterisation of CuNPs: insights into their potential bio-activity. *IET Nanobiotechnol* 12:357–364
28. Nayak S, Kumar Khuntia S (2019) Development and study of properties of *Moringa oleifera* fruit fibers/polyethylene terephthalate composites for packaging applications. *Compos Commun* 15:113–119
29. Madubuonu N, Aisida SO, Ali A, Ahmad I, Zhao TK, Botha S, Maaza M, Ezema FI (2019) Biosynthesis of iron oxide nanoparticles via a composite of *Psidium guajava*-*Moringa oleifera* and their antibacterial and photocatalytic study. *J Photochem Photobiol B Biol* 199:111601
30. Kwaambwa HM, Maikokera R (2008) Infrared and circular dichroism spectroscopic characterisation of secondary structure components of a water treatment coagulant protein extracted from *Moringa oleifera* seeds. *Colloids Surf B Biointerfaces* 64:118–125
31. Swelam A, Saied S, Hafez A (2019) Removal comparative study for Cd(II) ions from polluted solutions by adsorption and coagulation techniques using *Moringa oleifera* seeds. *Egypt J Chem* 62:1499–1517
32. Prasuna CPL, Chakradhar RPS, Rao JL, Gopal NO (2009) EPR and IR spectral investigations on some leafy vegetables of Indian origin. *Spectrochim Acta A Mol Biomol Spect* 74:140–147
33. Bello OS, Adegoke KA, Akinyunni OO (2017) Preparation and characterization of a novel adsorbent from *Moringa oleifera* leaf. *Appl Water Sci* 7:1295–1305
34. Kebede TG, Dube S, Nindi MM (2018) Fabrication and characterization of electrospun nanofibers from *Moringa stenopetala* seed protein. *Mater Res Express* 5:125015
35. Kebede TG, Dube S, Nindi MM (2019) Characterisation of water-soluble protein powder and optimisation of process parameters for the removal of sulphonamides from wastewater. *Environ Sci Pollut Res* 26:21450–21462
36. Bhutada PR, Jadhav AJ, Pinjari DV, Nemade PR, Jain RD (2016) Solvent assisted extraction of oil from *Moringa oleifera* Lam seeds. *Ind Crops Prod* 82:74–80
37. Finzi-Quintão CM, Novack KM, Bernardes-Silva AC, Silva TD, Moreira LE, Braga LE (2018) Influence of *Moringa oleifera* derivatives in blends of PBAT/PLA with LDPE. *Polímeros* 28:309–318
38. Ferreira FV, Dufresne A, Pinheiro IF, Souza DH, Gouveia RF, Mei LH, Lona LM (2018) How do cellulose nanocrystals affect the overall properties of biodegradable polymer nanocomposites: a comprehensive review. *Eur Polym J* 108:274–285
39. Leal IL, da Silva Rosa YC, da Silva PJ, Cruz Correia PR, da Silva MP, Guimarães DH, Barbosa JD, Druzian JI, Machado BA (2019) Development and application starch films: PBAT with additives for evaluating the shelf life of Tommy Atkins mango in the fresh-cut state. *J Appl Polym Sci* 136:48150
40. Dou Q, Cai J (2016) Investigation on polylactide (PLA)/poly(butylene adipate-co-terephthalate) (PBAT)/bark flour of plane tree (PF) eco-composites. *Materials* 9:393
41. He H, Liu B, Xue B, Zhang H (2019) Study on structure and properties of biodegradable PLA/PBAT/organic-modified MMT nanocomposites. *J Thermoplas Compos Mater* 6:0892705719890907
42. Pinheiro IF, Ferreira FV, Souza DH, Gouveia RF, Lona LM, Morales AR, Mei LH (2017) Mechanical, rheological and degradation properties of PBAT nanocomposites reinforced by functionalized cellulose nanocrystals. *Eur Polym J* 97:356–365
43. Cheng M, Wang J, Zhang R, Kong R, Lu W, Wang X (2019) Characterization and application of the microencapsulated carvacrol/sodium alginate films as food packaging materials. *Int J Biol Macromol* 141:259–267
44. Moustafa H, Guizani C, Dupont C, Martin V, Jeguirim M, Dufresne A (2017) Utilization of torrefied coffee grounds as reinforcing agent to produce high-quality biodegradable PBAT composites for food packaging applications. *ACS Sustain Chem Eng* 5:1906–1916
45. Wu CS (2012) Utilization of peanut husks as a filler in aliphatic-aromatic polyesters: preparation, characterization, and biodegradability. *Polym Degrad Stab* 97:2388–2395
46. Rahimi SK, Aeinehvand R, Kim K, Otaigbe JU (2017) Structure and biocompatibility of bioabsorbable nanocomposites of aliphatic-aromatic copolyester and cellulose nanocrystals. *Bio-macromol* 18:2179–2194
47. Buffa JM, Mondragon G, Corcuera MA, Eceiza A, Mucci V, Aranguren MI (2018) Physical and mechanical properties of a vegetable oil based nanocomposite. *Eur Polym J* 98:116–124
48. Zhang X, Ma P, Zhang Y (2016) Structure and properties of surface-acetylated cellulose nanocrystal/poly(butylene adipate-co-terephthalate) composites. *Polym Bull* 73:2073–2085
49. Moustafa H, Guizani C, Dufresne A (2017) Sustainable biodegradable coffee grounds filler and its effect on the hydrophobicity, mechanical and thermal properties of biodegradable PBAT composites. *J Appl Polym Sci* 134:1–11
50. Mukherjee T, Tobin MJ, Puskar L, Sani MA, Kao N, Gupta RK, Pannirselvam M, Quazi N, Bhattacharya S (2017) Chemically imaging the interaction of acetylated nanocrystalline cellulose (NCC) with a polylactic acid (PLA) polymer matrix. *Cellulose* 24:1717–1729
51. Meng D, Xie J, Waterhouse GI, Zhang K, Zhao Q, Wang S, Qiu S, Chen K, Li J, Ma C, Pan Y (2019) Biodegradable Poly(butylene adipate-co-terephthalate) composites reinforced with bio-based nanochitin: preparation, enhanced mechanical and thermal properties. *J Appl Polym Sci* 137:48485
52. Venkatesan R, Rajeswari N (2017) ZnO/PBAT nanocomposite films: investigation on the mechanical and biological activity for food packaging. *Polym Adv Technol* 28:20–27
53. Falcão GA, Vitorino MB, Almeida TG, Bardi MA, Carvalho LH, Canedo EL (2017) PBAT/organoclay composite films: preparation and properties. *Polym Bull* 74:4423–4436
54. Arfat YA, Ahmed J, Ejaz M, Mullah M (2018) Polylactide/graphene oxide nanosheets/clove essential oil composite films for potential food packaging applications. *Int J Biol Macromol* 107:194–203
55. Liu Y, Wang S, Lan W, Qin W (2017) Fabrication and testing of PVA/chitosan bilayer films for strawberry packaging. *Coatings* 7:109
56. Siripatrawan U, Vitchayakitti W (2016) Improving functional properties of chitosan films as active food packaging by incorporating with propolis. *Food Hydrocoll* 61:695–702
57. Liu Y, Wang S, Lan W (2018) Fabrication of antibacterial chitosan-PVA blended film using electrospray technique for food packaging applications. *Int J Biol Macromol* 107:848–854

58. da Silva IS, Neto WP, Silvério HA, Pasquini D, Zeni Andrade M, Otaguro H (2017) Mechanical, thermal and barrier properties of pectin/cellulose nanocrystal nanocomposite films and their effect on the storability of strawberries (*Fragaria ananassa*). *Polym Adv Technol* 28:1005–1012
59. Giuggioli NR, Girgenti V, Briano R, Peano C (2017) Sustainable supply-chain: evolution of the quality characteristics of strawberries stored in green film packaging. *CYTA J Food* 15:211–219
60. Zhong Y, Godwin P, Jin Y, Xiao H (2019) Biodegradable polymers and green-based antimicrobial packaging materials: a mini-review. *Adv Ind Eng Polym Res* 3:27–35
61. Maqsood M, Qureshi R, Arshad M, Ahmed MS, Ikram M (2017) Preliminary phytochemical screening, antifungal and cytotoxic activities of leaves extract of *Moringa oleifera* lam. From salt range, Pakistan. *Pak J Bot* 49:353–359
62. Jimoh WA, Ayeloja AA, Badmus GO, Olateju KO (2020) Antibacterial and antifungal effect of moringa (*Moringa oleifera*) seedmeal on marinated smoked African mud catfish (*Clarias gariepinus*). *J Food Saf* 4:e12772
63. Valenzuela C, Tapia C, López L, Bunge A, Escalona V, Abugoch L (2015) Effect of edible quinoa protein-chitosan based films on refrigerated strawberry (*Fragaria × ananassa*) quality. *Electron J Biotechnol* 18:406–411